Ann. Biomed. Eng. manuscript No.
(will be inserted by the editor)

Effect of eddy length scale on mechanical loading of blood cells in turbulent flow

Patrick N. Dooley *, Nathan J. Quinlan

National Centre for Biomedical Engineering Science and Department of Mechanical and Biomedical Engineering, National University of Ireland Galway, Ireland

e-mail: nathan.quinlan@nuigalway.ie

Received: date / Revised version: date

Abstract Non-physiological turbulent blood flow is known to occur in and near implanted cardiovascular devices, but its effects on blood are poorly understood. The objective of this work is to investigate the effect of turbulent eddy length scale on blood cell damage, and in particular to test the hypothesis that only eddies similar in size to blood cells can cause damage. The microscale flow near a red blood cell (RBC) in an idealized turbulent eddy is modelled computationally using an immersed boundary method. The model is validated for the special case of a tank-treading RBC. In comparisons between turbulent flow fields, based on Kolmogorov theory, the model predicts that damage due to the smallest eddies is almost inde-

* Present address: MCS, Galway Technology Park, Parkmore, Galway, Ireland
Correspondence to: Nathan J. Quinlan

pendent of the Kolmogorov length scale. The model predicts that within a given flow field, however, eddies of sub-cellular scale are less damaging than larger eddies. Eddy decay time and the turbulent energy spectral density are highlighted as important factors. The results suggest that Kolmogorov scale is not an adequate predictor of flow-induced blood trauma, and highlights the need for deeper understanding of the microscale structure of turbulent blood flow.

Introduction

Turbulent blood flow occurs near implanted cardiovascular devices such as mechanical heart valves (MHVs) that interact with blood flowing at high Reynolds number, and can cause blood damage[39] as a result of the abnormal mechanical loading of blood cells by flow in their microscale surroundings. Turbulent flow is characterized by flow structures (eddies) over a wide spectrum of length scales. However, little is known about the structure and effects of turbulence at the cellular scale, and direct microscopic experimental study of turbulent blood flow is not currently feasible. There is a need for better understanding of the mechanisms of cell damage by turbulent eddy structures at the microscale. In this study, a computational model is used to simulate the interaction between a blood cell and an idealized turbulent eddy, and to evaluate the influence of turbulent eddy length scales on mechanical loading of blood cells.

Knowledge of the microscale flow field is necessary to fully understand the causes of both hemolysis and thrombosis in turbulent flow. In the present work, attention is restricted to hemolysis and the red blood cell (RBC), although the principles are equally applicable to thrombosis. Studies have shown that the RBC membrane is most susceptible to rupture by areal extension of the membrane, when the isotropic tension (defined as the force per unit width of the two-dimensional membrane surface) exceeds a critical threshold.[9,22,31] In a micropipette experiment, Evans *et al.*[9] measured the threshold isotropic tension beyond which membrane rupture occurs as 10 mN/m, corresponding to an areal strain of 2–3 %. The RBC membrane can withstand large uniaxial membrane strains without rupturing.[10] The threshold bulk viscous shear stress in laminar flow required to lyse RBCs, measured in *in vitro* experiments, ranges from 150 - 560 Pa.[15,20,38]

Kameneva *et al.*[18] confirmed directly that the mechanisms of flow-induced hemolysis are fundamentally different in laminar and turbulent flows. Turbulent pipe flow at a Reynolds number of 5100 was shown to result in higher hemoglobin release (by a factor of 6) than laminar flow at the same mean wall shear stress with a Reynolds number of 1000. The additional trauma could only result from the loading of cells by turbulent eddies. This experiment confirms the importance of the structure of turbulent blood flow to turbulence-induced blood damage.

Kolmogorov theory has been used to estimate the size of the smallest (energy-dissipating) eddies in a measured turbulent flow. For measured

MHV flows, reported values of Kolmogorov length scale are 7 μm in hinge flow,[8] 36–72 μm for leakage jets *in vivo*,[36] and 25–47 μm in forward flow.[21] These results suggest that cardiovascular device flows may contain eddies of size comparable to a red blood cell (diameter 8 μm). However, Kolmogorov theory is based on assumptions of isotropic, homogeneous, statistically stationary turbulence. Sutera and Joist,[34] among others, have pointed out that these conditions do not hold in the short-duration pulsatile flow through a MHV, and it is not known to what extent Kolmogorov theory is applicable in this regime. It has been suggested[1,8,18,23] that smaller turbulent eddies are more damaging to blood cells, but there is no direct evidence to support this hypothesis.

Reynolds stress has been widely used as a parameter to characterize turbulence and to predict flow-induced trauma in hemodynamic flow fields.[8,14,21,33] However, the Reynolds stress is an averaged momentum flux which contains no information about the size of flow structures in turbulence, and therefore cannot fully characterize the mechanical environment of individual cells. It has been shown that the Reynolds stress is an inaccurate indicator of true viscous stresses in turbulent flow of a homogeneous fluid,[13,17] and of flow-induced stress on blood cells suspended in turbulent flow.[30]

Quinlan and Dooley[30] calculated the approximate contribution to the flow-induced stress on blood cells from eddies across a spectrum of length scales, based on measurements by Liu *et al.*[21] of flow downstream of a MHV. The results showed that the viscous shear stress on cells is at least an order

of magnitude less than the Reynolds stress, and depends on the turbulent energy spectrum as well as the Reynolds stress. It was also shown that the smallest eddies in a turbulent flow are not necessarily the most damaging to cells. This analysis was based on a simplified model of a blood cell (as a rigid sphere), and was restricted in scope to turbulent eddies larger than the cell.

In the present study, the earlier work is extended to consider the interactions of deformable cells with flow structures of cellular size or smaller. A computational fluid-structure interaction technique is developed, validated for the special case of a tank-treading RBC, and used to simulate the flow-induced loading of flexible RBCs interacting with turbulent eddies in two dimensions. A turbulent eddy is idealized as a vortex defined by characteristic length and velocity scales, and the immersed boundary method[29] is used to compute the fluid-structure interaction. This method is used to test the hypothesis that the smallest turbulent eddies are most damaging to cells.

Method and Validation

The Immersed Boundary Method

The immersed boundary (IB) method is a mixed Eulerian-Lagrangian fluid-structure interaction (FSI) technique developed by Peskin[29] to simulate fluid-structure interactions in the heart. In computational modelling of the strong interactions of fluids with very flexible solids in biological systems, the

fluid-solid interface can become severely distorted. The IB method avoids the need for a body-fitted grid in the fluid domain by treating the solid surface as a boundary immersed in fluid. The solid is advected by the fluid flow, and the fluid and solid domains are discretized independently. The principle is illustrated in Fig. 1.

For a massless solid boundary Γ immersed in viscous incompressible fluid in a two-dimensional domain Ω, the Navier-Stokes equations governing fluid motion in Cartesian coordinates are

$$\nabla \cdot \mathbf{u} = 0 \tag{1}$$

$$\frac{\partial \mathbf{u}}{\partial t} + \mathbf{u} \cdot \nabla \mathbf{u} = \nu \nabla^2 \mathbf{u} + \frac{1}{\rho} \left(-\nabla p + \mathbf{f} \right), \tag{2}$$

and the equations governing the boundary-fluid interaction are

$$\mathbf{f}(\mathbf{x}, t) = \int_{\Gamma} \mathbf{F}'(s, t) \delta(\mathbf{x} - \mathbf{X}(s, t)) ds \tag{3}$$

$$\frac{\partial \mathbf{X}(s, t)}{\partial t} = \int_{\Omega} \mathbf{u}(\mathbf{x}, t) \delta(\mathbf{x} - \mathbf{X}(s, t)) d\mathbf{x}. \tag{4}$$

Here $\mathbf{x}$ is a point in the fluid domain, $\delta(\mathbf{x})$ is the Dirac delta function, $\mathbf{u}(\mathbf{x}, t)$ is the fluid velocity field, $\nu(\mathbf{x}, t)$ is the kinematic viscosity, and $p(\mathbf{x}, t)$ is the fluid pressure. $\mathbf{X}(s, t)$ is the location of a point on Γ as a function of time t and the coordinate s, which parameterizes the boundary curve. The force density (force per unit area for the present 2D application) transmitted from the solid to the fluid is $\mathbf{f}(\mathbf{x}, t)$, and the corresponding force density per unit boundary length is $\mathbf{F}'(\mathbf{X}(s, t), t)$. Equation (3) enforces equilibrium at the interface between the fluid and solid phases, and Eq. (4) expresses

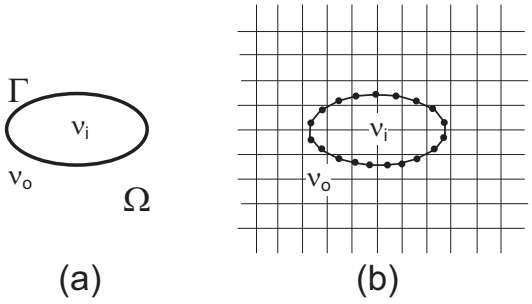

Fig. 1 (a) Immersed solid boundary Γ in fluid domain Ω. Different fluid properties (described by the fluid kinematic viscosity ν) are defined on each side of the boundary. (b) Spatial discretization of solid by a Lagrangian grid and fluid by a fixed Cartesian grid.

the continuity of the velocity field between fluid and solid (required by the no-slip condition).

To construct a practical discrete method, the boundary is discretized by one-dimensional Lagrangian line elements, and the fluid domain is discretized by a Eulerian grid, as shown in Fig. 1(b). The distributed boundary force $\mathbf{F}'(\mathbf{X}(s,t),t)$ is replaced with a set of discrete forces $\mathbf{F}_i$ at the Lagrangian nodes, representing out-of-balance internal forces in the boundary structure. $\mathbf{F}_i$ is given by

$$\mathbf{F}_i = T_i\mathbf{e}_i - T_{i-1}\mathbf{e}_{i-1}, \tag{5}$$

where the subscripts $i-1$ and i denote adjacent line elements which share the node i, $\mathbf{e}$ are the unit tangent vectors along them, and T is the element tension. As in the front-tracking method of Unverdi and Tryggvason[37], the boundary separates fluids with different values of viscosity. The singu-

lar Dirac delta functions are replaced with the following two-dimensional smoothed approximation given by Peskin:[29]

$$D_h(\mathbf{x}-\mathbf{X}(s,t)) = \begin{cases} \frac{1}{16h^2}\prod_{k=1}^{2}\left(1+\cos\frac{\pi r^k}{2h}\right) & : \quad r^k \leq 2h \\ 0 & : \quad \text{otherwise}, \end{cases} \tag{6}$$

where $r^k = \left|x^k - X^k\right|$ with $k = 1, 2$ denoting coordinate indices, and h is the uniform spacing of the fluid grid. The integrals in Eqs. (3–4) are then replaced with discrete sums

$$\mathbf{f}_j = \sum_i D_h(\mathbf{x}_j - \mathbf{X}_i)\mathbf{F}_i \tag{7}$$

$$\mathbf{u}_i = \sum_j D_h(\mathbf{x}_j - \mathbf{X}_i)\mathbf{u}_j, \tag{8}$$

where i and j represent the Lagrangian (solid) and Eulerian (fluid) grid points, respectively. In this framework, Eq. (7) defines a distribution of interaction forces from the solid boundary nodes to neighbouring fluid nodes, and Eq. (8) may be interpreted as an interpolation of the velocity field from the fluid to the solid. The latter step ensures continuity of the fluid and solid velocity fields and enforcement of the no-slip condition.

Red Blood Cell Model

The RBC is modelled in two dimensions as a circular elastic membrane of diameter $2a = 8$ μm. The membrane separates blood plasma with kinematic viscosity $\nu_o = 1.2\times10^{-6}$ m^2/s from internal cytoplasmic fluid with viscosity $\nu_i = 5.8 \times 10^{-6}$ m^2/s. The elastic tension T in the membrane is given by

the constitutive equation due to Hochmuth and Waugh[16]:

$$T = \frac{\mu}{2}\left(\lambda^2 - \lambda^{-2}\right), \tag{9}$$

where μ denotes the shear modulus of the membrane and λ is the membrane extension ratio. μ is taken as 6×10^{-3} mN/m.[16]

Numerical Implementation

The model was implemented in the OpenFOAM 1.4 open-source CFD package.[28] The Navier-Stokes equations were solved using the PISO (pressure implicit with splitting of operators) algorithm for incompressible flow. The temporal terms in the Navier-Stokes equations were discretized using an implicit Euler scheme, and the temporal IB term in Eq. (4) was discretized using a first-order explicit scheme. The mesh density for both the solid and fluid domains was increased until a mesh-insensitive solution was achieved. For the results that follow, simulations were carried out using a 240×240 fluid grid, with 180 membrane nodes.

Validation of Red Blood Cell Model

Tank-treading of a RBC was simulated to validate the numerical model against the experimental results of Fischer *et al.*[12] and Fischer[11] and the analytical results of Tran-Son-Tay *et al.*[35] When a normal RBC is subjected to shear flow, it elongates and orients itself obliquely to the flow, and the membrane orbits in a tank-tread-like manner. The geometry and boundary

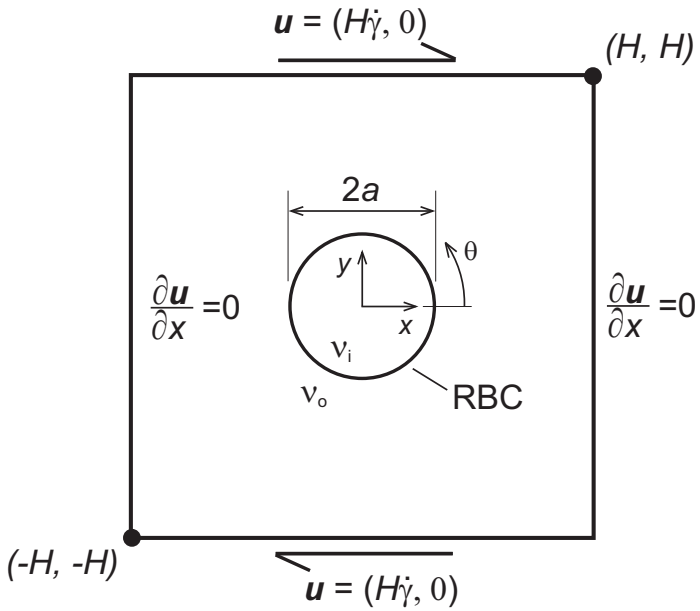

Fig. 2 Geometry and boundary conditions for simulation of RBC tank-treading. Dimensions are $D = 2a = 8$ μm and $H = 5a$.

conditions for this simulation are shown in Fig. 2. A known mean shear rate is imposed by prescribing equal and opposite wall velocities on the high and low y boundaries. Zero axial gradient of velocity is prescribed at the high and low x boundaries.

A simulation was carried out with external kinematic viscosity $\nu_o = 10^{-5}$ m^2/s, corresponding to the lower end of the viscosity range of non-physiological suspending media used in experiments by Fischer *et al.* The simulation resulted in a normalized tank-treading frequency $f_t/\dot{\gamma} = 0.029$, which is in good agreement with the values of approximately 0.024 and 0.025 reported by Fischer[11] and Fischer *et al.*[12] respectively.

Computations of membrane stress were validated by comparison with the analytical calculations of Tran-Son-Tay *et al.* ,[35] who modelled a tank-treading RBC as a three-dimensional ellipsoidal fluid-filled elastic capsule. The model allows membrane tension to be predicted as a function of deformed cell dimensions, cell orientation, membrane tank-treading frequency, and mean cytoplasmic overpressure. The mean cytoplasmic overpressure $\overline{\Delta p}$ (the pressure difference across the membrane) was estimated by Tran-Son-Tay *et al.* in a separate calculation, and the other variables were determined from experimental observations. An IB simulation (which does not require *a priori* knowledge of the above parameters) was carried out with external viscosity $\nu_o = 1.2 \times 10^{-6}$ m^2/s and mean shear rate $\dot{\gamma}$ of 286 s^{-1}, corresponding to a value used by Tran-Son-Tay *et al.*[35] The predicted membrane geometry, membrane velocity, and mean overpressure were then used as input to analytical calculations based on the method of Tran-Son-Tay *et al.* As shown in Fig. 3, the initially circular membrane is predicted to approach an inclined, approximately elliptical shape in steady state. The predicted pressure field is highly non-uniform, with the cytoplasmic overpressure Δp ranging from 0.56 to 1.24 Pa. The frequency of the tank-tread motion f_t in this simulation is approximately 6.9 s^{-1}, corresponding to $f_t/\dot{\gamma} = 0.024$.

Membrane tension computed by the IB model and the analytical model are compared in Fig. 4. There is good agreement for peak tension. However, the IB method predicts regions of negative membrane tension (compression), while the analytical model predicts that the membrane is in tension

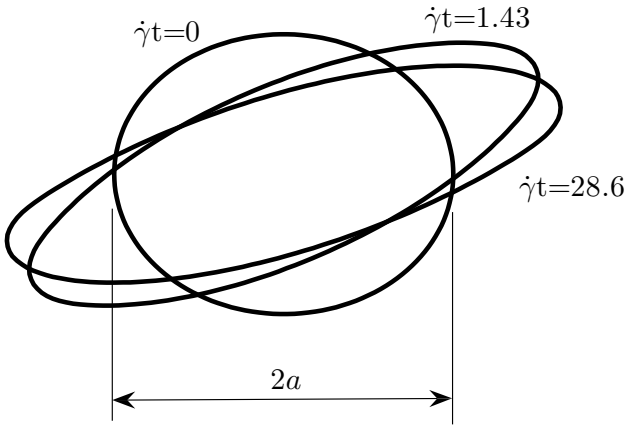

Fig. 3 Evolution of the RBC membrane under uniform shear of $\dot{\gamma} = 286$ s^{-1}, simulated using the immersed boundary method. By dimensionless time $\dot{\gamma}t = 28.6$ the tank-treading shape is close to steady state.

everywhere. This may be a consequence of the assumed uniaxial membrane loading in the two-dimensional IB numerical model, in contrast with bi-axial loading in the analytical model, as well as the non-uniform pressure in the IB model. However, the results confirm that the immersed boundary RBC model predicts the mechanical state of a RBC under flow-induced loading to sufficient accuracy for the purposes of the present study.

Application to Turbulent Flow

The subject of this study is the interaction of an isolated RBC with an idealized microscale turbulent eddy, characterized by a length and velocity

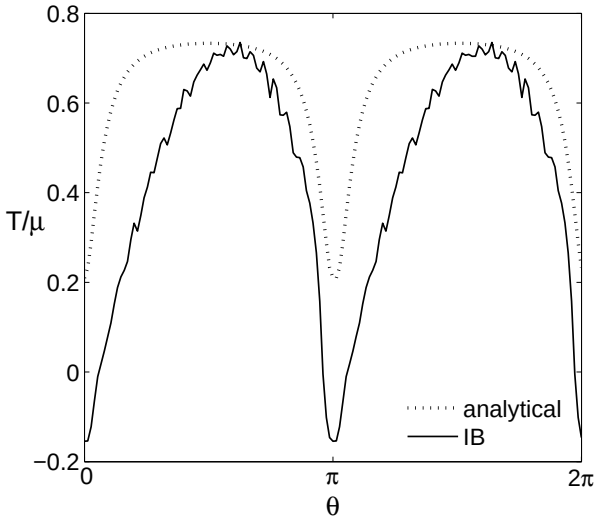

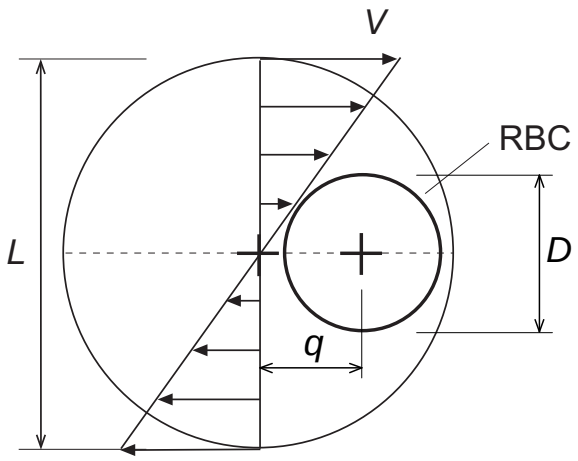

Fig. 5 Initial velocity field and cell positioning in an idealized turbulent eddy.

scale. The idealized eddy is initialized in the simulation as a circular region of diameter L, rotating as a rigid body with maximum tangential velocity V at its circumference, as shown in Fig. 5. Velocity is initially zero outside this region. Simulations were carried out for cells initially located at the eddy centre, outside the eddy, and at a range of intermediate positions between. The initial offset of the cell centre from the eddy centre is defined as q. The model represents the smallest eddies in a turbulent flow, which are created by the cascade of energy from larger length scales, and give up their kinetic energy through viscous dissipation.[2] It is therefore realistic to prescribe the initial condition of the eddy and allow it to decay while it interacts with the cell membrane. For the present purposes, it is not necessary to consider the process of creation of these eddies, except to determine the characteristic length and velocity scales L and V, which define the initial conditions for the microscale flow field.

Two approaches are used here to estimate realistic initial conditions. The first is a comparison of the effects of the smallest eddies (according to Kolmogorov theory) in different flow fields. In the second approach, experimental data from the literature are used to model the effects of various eddies in a single flow. Both approaches are performed for length scales spanning an order of magnitude around cellular scale, with L = 4, 10, 20, and 40 μm.

The first approach is based on the Kolmogorov length and velocity scales, η and V_d, which are theoretical estimates of characteristic scales of the

smallest eddies in statistically stationary, homogeneous, isotropic turbulent flow. They are functions only of kinematic viscosity ν and energy dissipation rate ε, and are given by[3,5]

$$\eta = \left(\frac{\nu^3}{\varepsilon}\right)^{1/4} \tag{10}$$

and

$$V_d = (\nu\varepsilon)^{1/4}\,. \tag{11}$$

Therefore, the Kolmogorov velocity and length scales are related by

$$V_d = \frac{\nu}{\eta}. \tag{12}$$

For plasma kinematic viscosity of $\nu = 1.2 \times 10^{-6}$ m^2/s, the length scales L = 4, 10, 20, and 40 μm correspond to velocity scales of 0.29, 0.12, 0.059, and 0.029 m/s, respectively. These parameters were used to initialize the flow field as described above.

In the second approach, the *in vitro* experimental data of Liu *et al.*[21] were used to determine initial length and velocity scales of model turbulent eddies. Liu *et al.* measured the turbulent energy spectrum downstream of a MHV using laser Doppler velocimetry (LDV). Figure 6 shows the normalized energy spectral density $E/\overline{u'^2}$ at peak systole. The data can be represented by a piecewise power law with exponents 0.30, -2.03, and -1.03. The 0.30 and -2.03 exponents correspond to the turbulence-producing and inertial subranges, respectively.[3,5] However, the change of exponent from -2.03 to -1.03 is difficult to explain in physical terms, and is likely to be an artifact due to the well-known particle-rate filter effect in LDV (demonstrated,

for example, by Nobach *et al.*[27]). Therefore, we reject the high-frequency portion of the power law.

Liu *et al.* reported a broad turbulent spectrum around the middle of the pre-systole flow acceleration period (in addition to the data for peak systole used here). This contrasts with particle image velocimetry (PIV) by Dasi *et al.*[6] which shows quite clearly that flow is laminar around that time, with no apparent structures smaller than vortices of diameter about 2 mm (the PIV interrogation window size was 133 μm and the light-sheet thickness approximately 200 μm). This discrepancy may be at least partly explained by the fact that the measurements by Liu *et al.* were conducted at a higher Reynolds number (over 9000) than those of Dasi *et al.* (5960). While there is clearly a need for improved high-resolution experimental data, and recent PIV results represent a significant advance, the data of Liu *et al.* remain the most complete and direct measurement of a turbulent energy spectrum in a MHV flow.

Taylor's frozen-field hypothesis[3,5] can be used to estimate eddy length scales from measured spectral data of this kind. According to Taylor's hypothesis, for low turbulence intensity, turbulent eddies change relatively slowly as they are convected at the mean velocity U. Then the frequency f of velocity fluctuations is related to the size L of the turbulent eddies by $f \simeq U/L$. The mean velocity U reported by Liu *et al.*[21] is 1.69 m/s, and the root mean square velocity fluctuation $(\overline{u'^2})^{1/2}$ is 0.20 m/s, giving a turbulence intensity $(\overline{u'^2})^{1/2}/U$ of 12%, at which Taylor's hypothesis should

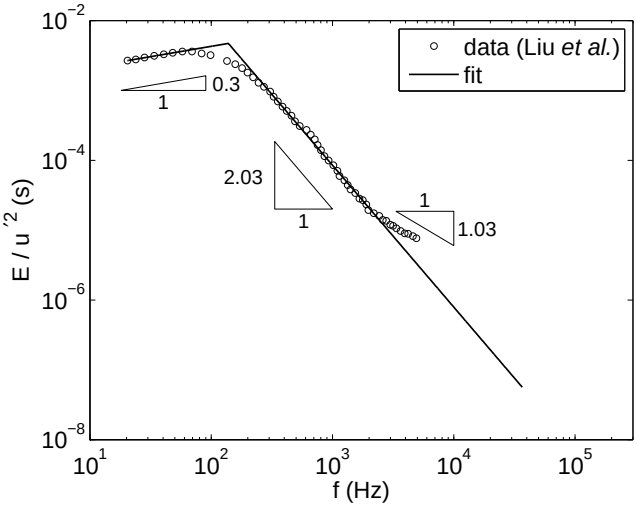

Fig. 6 Normalized energy spectral density for flow on the centerline 7.8 mm downstream of a St. Jude Medical bileaflet valve at peak flow, measured by Liu *et al.* using LDV.

hold to the accuracy required for this analysis. For this flow, a 4 μm eddy corresponds to a frequency of approximately 423 kHz. Due to signal processing and instrumentation limitations, Liu *et al.* reported spectral data for frequencies only up to 5 kHz. The spectrum is extrapolated to higher frequencies using the -2.03 exponent, to allow details of the microscale eddies to be calculated. This exponent is chosen rather than the exponent of -1.03 which fits the high-frequency range of the spectrum, because of the likely experimental artifact.

The energy spectral density $E(f)$ of a turbulent velocity signal $u(t)$ is defined such that $E(f)df$ is the infinitesimal contribution from fluctuations in a frequency band df centered on f to the total fluctuation energy $\overline{u'^2}/2$

(equal to half the mean square velocity fluctuation). Therefore, $E(f)$ is proportional to the square root of velocity fluctuations at f. For a spectrum represented by a power-law (as in this case) with exponent n, the characteristic velocity scale $V(f)$ of turbulent eddies varies according to

$$V \propto f^{\frac{n}{2}} \propto \left(\frac{U}{L}\right)^{\frac{n}{2}} \tag{13}$$

(making use again of Taylor's hypothesis).

This relation allows ratios of velocity scales at different frequencies to be determined, but does not give absolute velocity scales. An absolute velocity scale for fluctuations at some frequency f (and corresponding length scale $L = U/f$) can be determined by considering the mean square of velocity fluctuations at frequencies over a band of finite width Δf, centered on f. This is equivalent to an assumption that all of the energy in a band, $\int E(f)df \approx E(f)\Delta f$, is concentrated in a single eddy in one event. This is reasonable because the turbulent spectrum represents a statistical aggregation of many turbulent events, rather than a continuous distribution. However, the band width Δf must be chosen arbitrarily. The present work is concerned only with comparisons of the effects of turbulent structures at different length scales. For the simulations presented here, it was found that the relevant comparisons are independent of the choice of Δf for the range 1 Hz $\lesssim \Delta f \lesssim$ 10 kHz. This linear behaviour is to be expected, because the Reynolds number for plasma flow relative to a blood cell is in the range $10^{-5} < Re < 10^{-2}$ for the conditions tested. The results presented here have been obtained with $\Delta f = 10$ kHz and normalized with respect to Δf.

Results

Figures 7(a) and 7(b) show instantaneous fluid velocity fields and deformations of RBC membranes for cells in 4 μm and 20 μm Kolmogorov eddies. The results indicate that the sub-cellular eddy deforms a small portion of the RBC membrane, but that the larger eddy deforms the whole membrane, elongating and also transporting the cell.

In Fig. 8, maximum membrane tension is plotted as a function of time and initial cell position for four eddies of initial length scale from 4 to 40 μm, with corresponding velocity scale determined from Kolmogorov theory, as explained above. In these plots, tension is non-dimensionalised with respect to the membrane shear modulus μ. For all eddy length scales, the maximum membrane tension occurs when some part of the cell lies on the initial periphery of the eddy (i.e. in the range $1 - D/L \leq 2q/L \leq 1 + D/L$). Each curve in Fig. 8(b) represents the initial cell position which results in maximum tension for the corresponding eddy length scale. According to these results, the peak membrane tension induced by the Kolmogorov eddy is nearly independent of the eddy length scale.

Figure 9 shows the corresponding results for microscale eddies with velocity scales determined from the turbulent energy spectrum of Liu *et al.*[21]. In this modelling approach, the energy associated with an eddy is calculated by integrating the turbulent energy spectrum over a frequency band of small but arbitrary width Δf. The resulting tension T is approximately proportional to this width. Membrane tension is therefore presented in the

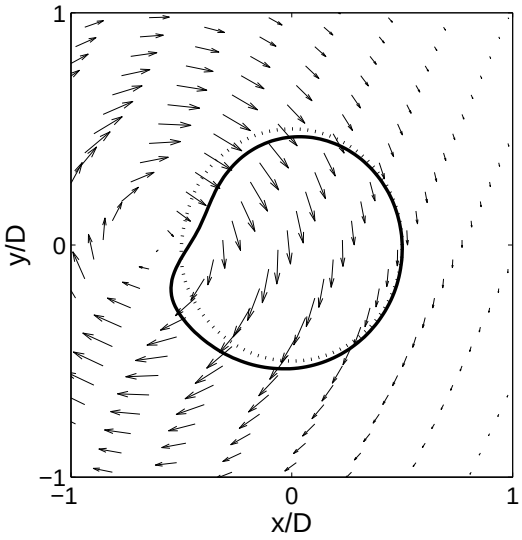

(a)

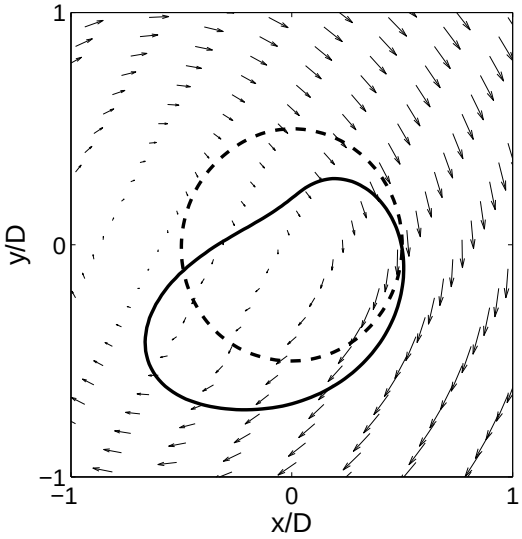

(b)

Fig. 7 Initial (**- -**) and deformed (—) shape of a RBC membrane interacting with (a) 4 μm and (b) 20 μm Kolmogorov eddies, with instantaneous fluid velocity fields. For clarity, the displacement of the membrane is scaled by a factor of 10.

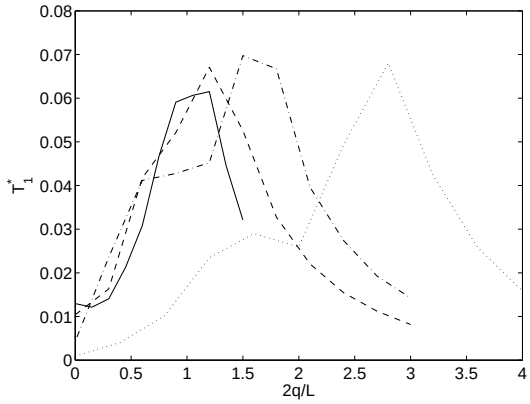

(a)

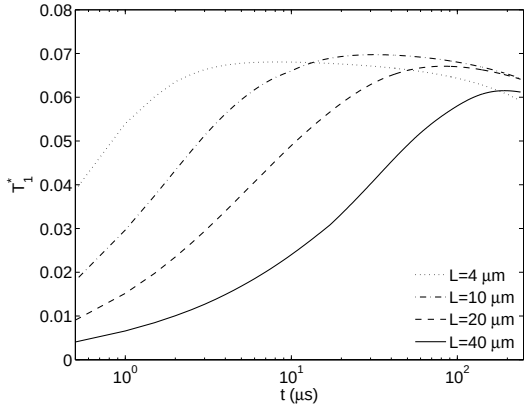

(b)

Fig. 8 Dimensionless membrane tension $T_1^* = T/\mu$ in a RBC in Kolmogorov eddies of length scale L from 4 to 40 μm. (a) Maximum tension as a function of initial cell position with respect to eddy. (b) Maximum instantaneous tension as a function of time, for the initial cell position resulting in the highest tension.

dimensionless form $T_2^* = T\nu/(\mu D^2 \Delta f)$, which is independent of Δf. Larger eddies induce greater peak values of membrane tension. This parameter is not directly comparable with T_1^* in Fig. 8. In this case, maximum membrane

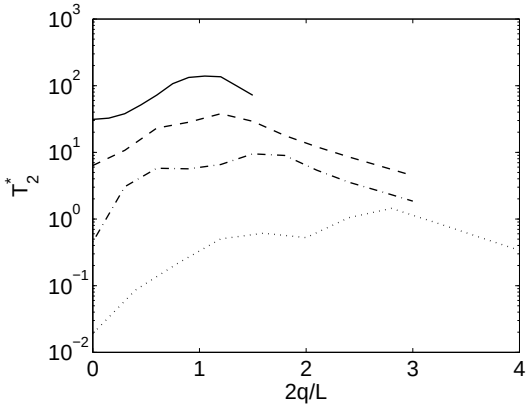

(a)

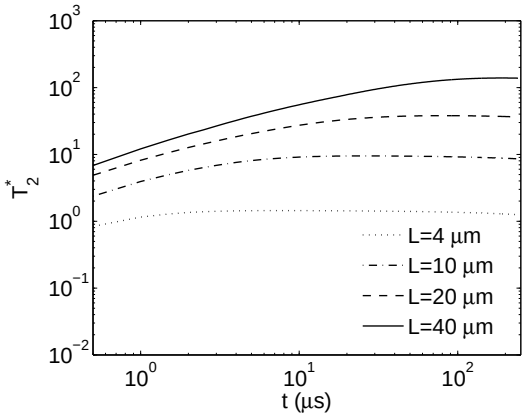

(b)

Fig. 9 Dimensionless membrane tension $T_2^* = T\nu/(\mu D^2 \Delta f)$ in a RBC in eddies of length scale L from 4 to 40 μm. Eddy velocity scales were calculated using the turbulent energy spectrum measured by Liu *et al.*[21] in turbulent flow downstream of a MHV. (a) Maximum tension as a function of initial cell position with respect to eddy. (b) Maximum instantaneous tension as a function of time, for the initial cell position resulting in the highest tension.

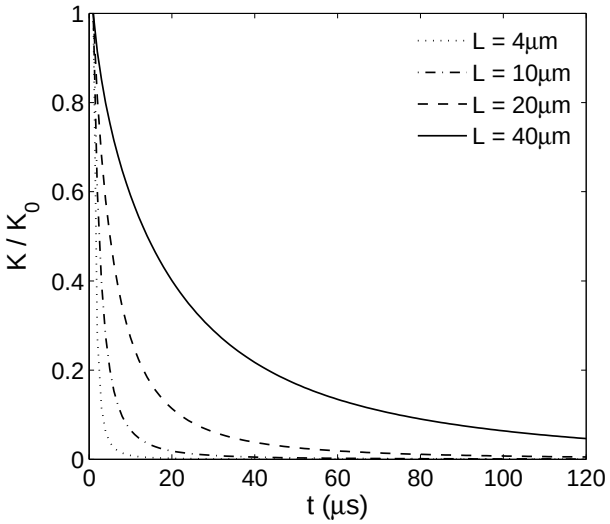

Fig. 10 Kinetic energy K as a function of time, normalized by initial energy K_0, for simulated decay of four eddies of initial length scale $L = 4$, 10, 20 and 40 μm, without a red blood cell.

tension increases with eddy length scale. The relationship is approximately quadratic.

Simulations were also carried out for flow in the absence of a red blood cell. Figure 10 shows the decay of total kinetic energy with time for eddies of length scale $L = 4$, 10, 20 and 40 μm. The decay of normalized kinetic energy is independent of the eddy's initial characteristic velocity, and hence independent of the the model (Kolmogorov theory or empirical data) used as a basis for the initial condition. The smallest eddies decay most rapidly.

Discussion

In this study, a two-dimensional immersed boundary method has been used to investigate the effect of the length scale of cellular-scale turbulent eddies on RBC membrane tension. An idealized structure was defined to model microscale turbulent eddies, and two approaches were used to determine characteristic length and velocity scales. This simple model realistically simulates the essential mechanical interactions between the plasma, cytoplasm and membrane.

Results based on Kolmogorov theory (Fig. 8) suggest that the smallest eddies in a flow cause a membrane tension which is independent of the size of those eddies (i.e. the Kolmogorov length scale). This finding calls into question the use of Kolmogorov length scale to assess potential for blood damage.

On the other hand, results based on the $E \propto f^{-2.03}$ spectrum (Fig. 9) indicate that small eddies cause lower stress than larger eddies. This indicates that the small, energy-dissipating eddies in a given flow field are not the prime cause of cellular blood damage. This is the primary result of the present work.

The two present approaches have fundamentally different meanings. The comparison between eddies of various Kolmogorov length and velocity scales is a comparison of different turbulent flows with different values of energy dissipation rate ε. On the other hand, the comparison based on a modified empirical turbulent spectrum represents a comparison of different scales in

a single flow field. This distinction is important in any discussion of the effects of turbulence length scales on suspended cells.

The interaction between a turbulent eddy and a suspended cell is a transient event. Referring to Figs. 8 and 9, flow-induced tension in the RBC membrane increases rapidly at first. The deformation of the membrane is resisted by viscous forces, internal elastic forces and the inertia of fluid which moves with it. Peak membrane tension occurs when these forces reach instantaneous equilibrium. This takes place within microseconds for a 4 μm eddy or about 100 μs for a 40 μm eddy, comparable with the time-scale of decay of a free eddy (Fig. 10). After this, the elastic forces in the membrane dominate, and the RBC returns to its unstressed state. Smaller eddies are shown to decay faster than larger eddies (Fig. 10), decreasing the exposure time of a cell to the eddy. This suggests that the transient dissipation of a small eddy plays a role in limiting the damage it may cause. The deformation of the cell during this process is small, as illustrated in Fig. 7.

In this study, the turbulent energy spectrum of Liu *et al.*[21] was extrapolated to higher frequencies using a power–law fit $E(f) \propto f^n$, with $n = -2.03$, to allow details of the microscale eddies to be calculated. As highlighted by Eq. (13), the analysis is dependent on the distribution of turbulent kinetic energy across frequencies, which in turn depends on the choice of n. Simulations have also been carried out with the widely accepted value $n = -5/3$, theoretically predicted and empirically confirmed for a wide range of turbulent flows,[32] and the qualitative conclusions are essentially the

same. Around frequencies corresponding to the smallest scales in a turbulent flow, turbulent energy spectra are better fitted by $E(f) \propto e^{-\alpha f}$.[4,24] This exponential decay in the distribution of energy across the high-frequency spectrum would increase the differentiation in cell loading at different eddy length scales, reinforcing the conclusions of this study.

Interactions between a single cell and a single eddy have been considered here. In reality, multiple eddies at cellular scale may occur near a cell simultaneously or sequentially. It is likely that complex additional phenomena occur in the interactions of multiple eddies (of different sizes) with multiple cells, and this is an important topic for future models.

The fluid-structure interaction model was validated by simulation of tank-treading and comparison with the model of Tran-Son-Tay *et al.*[35]. Good agreement was achieved for the value of peak tension and the qualitative distribution of tension over the cell, but regions of negative tension and low cytoplasmic pressure were predicted by the present model in regions where Tran-Son-Tay *et al.* predict small positive tension values ($\theta \approx 0, \pi$ in Figure 4). In a three-dimensional incompressible membrane (as modelled by Tran-Son-Tay *et al.*), extension in the plane of flow shear would result in out-of-plane membrane contraction and compressive force on the cell contents. The absence of this effect in the present two-dimensional model may explain the regions of low pressure and associated membrane compression. A fully three-dimensional model will be required to determine the effect of RBC membrane areal incompressibility.

This analysis does not address the fundamental question of whether cell-scale turbulent eddies exist. It is unclear whether the assumptions of homogeneous, isotropic, statistically stationary turbulence, on which Kolmogorov theory are based, apply in the brief peak flow through MHVs.[21,34] Even if Kolmogorov theory were valid for flow of a homogeneous fluid in cardiovascular conditions, it could not be expected to predict microscale flow in whole blood at physiological hematocrit, where interactions between cells and plasma must dominate the fluid mechanics. From recent experimental and computational results at the current technological limit of resolution,[6] it appears that the smallest flow structures in MHV flow may be orders of magnitude larger than cells, contrary to previous results based on Kolmogorov theory. There is a need for experimental measurements at still higher spatial resolution to shed more light on small-scale structure, and there is a complementary role for high-resolution direct numerical simulation to probe the microscale.

Conclusions

The mechanical loading of a red blood cell in turbulent eddies has been simulated computationally using a two-dimensional fluid-structure interaction model with a flexible cell membrane. Two approaches were used to define the local turbulent eddy structure. In the first approach, loading was compared across different turbulent flows, using Kolmogorov theory (following much of the literature in this field) to estimate the velocity scale of smallest

eddies as a function of their length scale. This model indicates that damage due to smallest eddies is independent of the Kolmogorov length scale. However, it remains an open question whether Kolmogorov theory is valid in highly unsteady cardiovascular flow. In the second approach, eddies of various scales were compared within a single turbulent flow field, based on experimental data. According to this model, the smallest eddies in a given turbulent flow field cause the least damage. This finding suggests that the Kolmogorov scale (the estimated size of the smallest eddies) is not the most important predictor of cell damage in turbulent blood flow. The distribution of energy across turbulence length scales and the time scale of turbulent eddies are highlighted as important influences on turbulence-induced blood trauma.

Acknowledgements Patrick N. Dooley gratefully acknowledges the support of the Irish Research Council for Science, Engineering and Technology, funded by the National Development Plan.

References

1. Baldwin, J. T., Deutsch, S., Petrie, H. L., Tarbell, J. M. Determination of principal Reynolds stresses in pulsatile flows after elliptical filtering of discrete velocity measurements. *J. Biomech. Eng.* 115:396–403, 1993.
2. Bernard, P. S., Wallace, J. M. Turbulent Flow Analysis, Measurement, and Prediction. New Jersey: John Wiley & Sons, 2002.

3. Bradshaw, P. An Introduction to Turbulence and its Measurement. Oxford: Pergamon Press, 1971.

4. Chen, S., Doolen, G., Herring, J. R., Kraichnan, R. H., Orzag, S. A., Su She, Z. Far-Dissipation Range of Turbulence. *Phys. Rev. Lett.* 70: 3051–3054, 1993.

5. Davidson, P. A. Turbulence: an introduction for scientists and engineers. Oxford: Oxford University Press, 2004.

6. Dasi, L. P., L. Ge., and H. A. Simon. Vorticity dynamics of a bileaflet mechanical heart valve in an axisymmetric aorta. *Phys. Fluids* 19:067105, 2007.

7. Eggleton, C. D., Popel, A. S. Large Deformation of Red Blood Cell Ghosts in a Simple Shear Flow *Phys. Fluids* 10:1834–1845, 1998.

8. Ellis, J. T., Wick, T. M., Yoganathan, A. P. Prosthesis-induced hemolysis: mechanisms and quantification of shear stress. *J. Heart Valve Dis.* 7:376–386, 1998.

9. Evans, E. A., Waugh, R., Melnik, L. Elastic area compressibility modulus of red cell membrane. *Biophys. J.* 16:585–595, 1976.

10. Evans E. A., P. L., La Celle Intrinsic material properties of the erythrocyte membrane indicated by mechanical analysis of deformation. *Blood* 45:29–43, 1975.

11. Fischer, T. M. Tank-tread frequency of the red cell membrane: dependence on the viscosity of the suspending medium. *Biophys. J.* 93:2553–2561, 2007.

12. Fischer, T. M., Stöhr-Liesen, M., Schmid-Schönbein, H. The red cell as a fluid droplet: tank tread-Like motion of the human erythrocyte membrane in shear flow. *Science* 202:894–896, 1978.

13. Ge, L., Dasi, L., Sotiropoulos, F., Yoganathan, A. J. Characterization of Hemodynamic Forces Induced by Mechanical Heart Valves: Reynolds vs. Viscous Stresses *Ann. Biomed. Eng.* 36:276-297, 2008.

14. Grigioni, M., Caprari, P., Tarzia, A., D'Avenio, G. Prosthetic heart valves' mechanical loading of red blood cells in patients with hereditary membrane defects. *J. Biomech.* 38:1557–1565, 2005.

15. Hellums, J. D., Brown, C. H. "Blood cell damage by mechanical forces." In: Cardiovascular Flow Dynamics and Measurements. Edited by N.H.C Hwang and N.A Normann. Baltimore: University Park Press 1977.

16. Hochmuth, R. M., Waugh, R. E. Erythrocyte Membrane Elasticity and Viscosity *Ann. Rev. Physiol.* 49:209–219, 1987.

17. Jones, S. A. A relationship between Reynolds stresses and viscous dissipation: implications to red cell damage. *Ann. Biomed. Eng.* 23:21–28, 1995.

18. Kameneva, M. V., Burgreen, G. W., Kono, K., Repko, B., Antaki, J. F., Umezu, M. Effects of turbulent stresses upon mechanical hemolysis: experimental and computational analysis. *Am. Soc. Artif. Intern. Organs J.* 50:418–423, 2004.

19. Kunas, K. T., Papoutsakis, E. T. Damage Mechanisms of Suspended Animal Cells in Agitated Bioreactors with and Without Bubble Entrain-

ment *Biotechnol. Bioeng.* 36:476–483, 1990.

20. Leverett, L. B., Hellums, J. D., Alfrey, C. P., Lynch, E. C. Red blood cell damage by shear stress. *Biophys. J.* 12:257–273, 1972.

21. Liu, J. S., Lu, P. C., Chu, S. H. Turbulence characteristics downstream of bileaflet aortic valve prostheses. *J. Biomech. Eng.* 122:118–124, 2000.

22. Lokhandwalla, M., Sturtevant, B. Mechanical haemolysis in shock wave lithotripsy (SWL): I. Analysis of cell deformation due to SWL flow-fields. *Phys. Med. Biol.* 46:413–437, 2001.

23. Lu, P. C., Lai, H. C., Liu, J. S. A reevaluation and discussion on the threshold limit for hemolysis in a turbulent shear flow. *J. Biomech.* 34:1361–1364, 2001.

24. Martínez, D. O., Chen, S., Doolen, G. D., Kraichnan, R. J., Wang, L. P., Zhou, Y. Energy Spectrum in the Dissipation Range of Fluid Turbulence *J. Plasma Phys.* 57:195–201, 1997.

25. Mecozzi, G., Milano, A. D., and De Carlo, M., Sorrentino, F., Pratali, S., Nardi, C., Bortolotti, U. Intravascular hemolysis in patients with new-generation prosthetic heart valves: A prospective study. *J. Thorac. Cardiovasc. Surg.* 123:550–556, 2002.

26. Niimi, H., Sugihara, M. Cyclic loading on the red cell membrane in a shear flow: a possible cause of hemolysis. *J. Biomech. Eng.* 107:91–95, 1985.

27. Nobach, H., Müller, E., Tropea, C. Efficient estimation of power spectral density from laser Doppler anemometer data. *Exp. Fluid* 24:499–509, 1998.

28. OpenCFD Limited, OpenFoam 1.4, (http://www.openfoam.org), 2007.

29. Peskin, C. S., Numerical analysis of blood flow in the heart. *J. Comput. Phys.* 25: 220–252, 1977.

30. Quinlan, J., Dooley, P. Models of Flow-Induced Loading on Blood Cells in Laminar and Turbulent Flow, with Application to Cardiovascular Device Flow *Ann. Biomed. Eng.* 35:1347–1356, 2007.

31. Rand, R. P., Burton, A. C. Mechanical properties of the red cell membrane: I. Membrane stiffness and intracellular pressure. *Biophys. J.* 4:115-135, 1964.

32. Saddoughi, S. G., Veeravalli, V. Local isotropy in turbulent boundary layers at high Reynolds number. *J. Fluid Mech.* 268:333–372, 1994.

33. Sallam, A. M., Hwang, N. H. C., Human red blood cells in a turbulent shear flow: contribution of Reynolds shear stresses. *Biorheology* 21:783–797, 1984.

34. Sutera, S.P., Joist, J. H. "Haematological Effects of Turbulent Blood Flow." In: Thrombosis, Embolism and Bleeding, edited by E.C. Butchart and E. Bodnar. London: ICR Publishers, 1992.

35. Tran-Son-Tay, R., Sutera, S. P., Zahalak, G. I., Rao, P.R. Membrane stress and internal pressure in a red blood cell freely suspended in a shear flow. *Biophys. J.* 51:915–924, 1987.

36. Travis, B. R., Leo, H. L., Shah, P. A., Frakes, D. H., Yoganathan, A. P. An analysis of turbulent shear stresses in leakage flow through a bileaflet mechanical prostheses. *J. Biomech. Eng.* 124:155–165, 2002.

37. Unverdi, S. O., Tryggvason, G. A Front-Tracking Method for Viscous Incompressible Multi-Fluid Flows. *J. Comput. Phys.* 100: 25–37, 1997.

38. Williams, A. R., Hughes, D. E., Nyborg, W. L. Hemolysis near a transversely oscillating wire. *Science* 169:871–873, 1970.

39. Yoganathan, A. P., Wick, T. M., Reul, H. "Influence of Flow Characteristics of Prosthetic Valves on Thrombus Formation." In: Thrombosis, Embolism and Bleeding, edited by E.C. Butchart and E. Bodnar. London: ICR Publishers, 1992.